Copy No. _____

Defence Research and Development Canada
Recherche et développement pour la défense Canada

DEFENCE R&D DÉFENSE

Numerical modelling of coherent broadband pulses for seismic exploration

John Fawcett

Defence R&D Canada – Atlantic

Technical Memorandum
DRDC Atlantic TM 2011-236
November 2011

Canada

This page intentionally left blank.

Numerical modelling of coherent broadband pulses for seismic exploration

John Fawcett

Defence Research and Development Canada – Atlantic
Technical Memorandum
DRDC Atlantic TM 2011-236
November 2011

Abstract

As part of the Offshore Energy Environmental Research (OEER)/DRDC Atlantic project "Feasibility of a Marine Vibroseis System to Minimize Potential Impacts of Seismic Surveying on Commercial Marine Invertebrates", DRDC Atlantic has been investigating the possibility and technical feasibility of using coherent broadband sources with complex waveforms (followed by matched-filtering) to replace high amplitude impulsive sources used in marine seismic surveys. This report discusses a MATLAB implementation of an acousto-elastic wavenumber algorithm for layered geoacoustic media. This code is then used to generate broadband time series for different geological configurations and incident waveforms. The relative performances of different impulsive and extended-time broadband sources are investigated. As well, the effects of the upper air/water interface and the inclusion of attenuations in the elastic layers are modelled.

Résumé

Dans le cadre d'un projet de l'association de recherche environnementale en énergie extracôtière (Offshore Energy Environmental Research - OEER) et de RDDC Atlantique portant sur la faisabilité d'un système vibrosismique marin visant à réduire au minimum les répercussions potentielles des études sismiques sur les invertébrés marins commerciaux, RDDC Atlantique a étudié la possibilité et la faisabilité technique de remplacer les sources impulsives à amplitude élevée utilisées dans les études séismiques marines par les sources à large bande cohérentes à formes d'ondes complexes (suivies d'un filtrage adapté). Le présent rapport porte sur l'intégration d'un code MATLAB à un algorithme de nombre d'ondes acousto élastique destiné à des milieux géoacoustiques en couches. Le code permettra ensuite de générer des séries chronologiques à large bande pour différentes configurations géologiques et formes d'onde incidentes. On a étudié les rendements relatifs de différentes sources à large bande impulsives et à durée étendue. On a également modélisé les répercussions de l'interface supérieure entre l'air et l'eau, ainsi que l'intégration d'affaiblissements aux couches élastiques.

This page intentionally left blank.

Executive summary

Numerical modelling of coherent broadband pulses for seismic exploration

John Fawcett; DRDC Atlantic TM 2011-236; Defence Research and Development Canada – Atlantic; November 2011.

Background: Typically in marine seismic exploration, large amplitude impulsive sources such as airgun arrays are used. There is concern as to the effects that such sound has on marine life including crustaceans. There is the possibility that one could used lower peak amplitude pulses that are extended over time and frequency (for example, a Chirp pulse) and regain the signal-to-noise ratio through coherent matched-filtering. This report describes an implementation of an acoustic/elastic model and examines the coherent matched-filtering of Chirp pulses for some examples. As well, a Ricker wavelet is used to represent a more impulsive type source.

Principal results: A MATLAB code was written to allow for the computation of seismic reflection time series at an array of receivers. The reflection time series for short-duration or extended-duration incident pulses were computed. It was found that an extended-duration pulse (after match-filtering) could yield seismic sections similar to that of a short-duration pulse given that the two pulses were approximately over the same frequency band. However, the polarity information which might be observed for the reflection of an impulsive wavelet is lost in the matched-filtered/envelope display. For higher-frequency sources the echo levels of deeper reflectors are reduced due to attenuation. Higher-bandwidth sources are able to better resolve thinner layers. The direct and surface-reflected pulses can significantly complicate the seismic section. In the case of match-filtering the sidelobes from these strong events could mask weak echoes.

Significance of results: The results show that extended (and lower peak amplitude) pulses may be used in seismic exploration. There are, of course, technical issues with constructing a coherent source with ample power in the frequency range corresponding to an airgun array. In the case that the coherent source is in a higher frequency band it is expected that the echoes from the deeper reflectors will suffer greater attenuation. Some care needs to be taken with the match-filtering so as to reduce the sidelobe levels. It is hoped that the MATLAB code developed in this report will be useful for further studies.

Future work: In future work we would like to continue our numerical simulations of seismic scenarios. In addition, the collection of real data to validate the numerical

modelling would be desirable.

Sommaire

Numerical modelling of coherent broadband pulses for seismic exploration

John Fawcett ; DRDC Atlantic TM 2011-236 ; Recherche et développement pour la défense Canada – Atlantique ; novembre 2011.

Contexte : En exploration sismique marine, on utilise généralement des sources d'impulsion à grande amplitude, comme des réseaux de canons à air. Toutefois, il existe certaines préoccupations quant aux effets de ceux-ci sur la vie marine, y compris les crustacés. Il est possible d'utiliser des impulsions à amplitude moins élevée qui sont étendues sur le plan du temps et des fréquences (p. ex. une impulsion modulée en fréquence), et de récupérer le rapport "signal sur bruit" au moyen d'un filtrage adapté cohérent. Dans le présent rapport, on décrit la mise en œuvre d'un modèle acousto élastique et étudie le filtrage adapté cohérent de quelques exemples d'impulsions modulée en fréquence. En outre, on utilise l'ondelette de Ricker pour représenter une source de type plus impulsive.

Résultats : On a développé un code MATLAB, afin de permettre de calculer les séries chronologiques de sismique réflexion d'un réseau de récepteurs, ainsi que les séries chronologiques de réflexion d'impulsions incidentes de courte et de longue durée. On a déterminé qu'une impulsion de longue durée (après un filtrage adapté) peut produire des coupes sismiques similaires à celles d'une impulsion de courte durée, car la bande de fréquences des deux impulsions est semblable. Toutefois, les données de polarisation observables lors de la réflexion d'une ondelette impulsive sont perdues dans l'affichage d'enveloppe ou de filtrage adapté. L'atténuation réduit les niveaux d'échos des réflecteurs plus profonds des sources à haute fréquence. Les sources à plus grande largeur de bande peuvent représenter plus facilement des couches minces. Les impulsions directes et réfléchies en surface peuvent compliquer considérablement la coupe sismique. Dans le cas d'un filtrage adapté, les lobes latéraux de ces fortes impulsions pourraient masquer de faibles échos.

Portée : Les résultats montrent que des impulsions étendues (et une amplitude plus basse) peuvent être utilisées en exploration sismique. Évidemment, la conception d'une source cohérente à haute puissance dont la gamme de fréquences correspond à celle d'un réseau de canons à air pose quelques problèmes techniques ; si la gamme de fréquences est plus élevée, on s'attend à ce que les échos des réflecteurs profonds subissent une atténuation plus forte. Il faut faire preuve d'une certaine rigueur pendant le filtrage adapté, afin de réduire les niveaux de lobes latéraux. On espère que le code MATLAB décrit dans le présent rapport s'appliquera à d'autres recherches.

Recherches futures : On souhaite continuer les simulations numériques de scénarios sismiques et acquérir des données réelles pour valider le modèle numérique.

Table of contents

List of figures

List of tables

Acknowledgements

I would like to thank Sean Pecknold for performing the OASES computations used in this report. Partial funding for this work was provided by Offshore Energy Environmental Research.

1 INTRODUCTION

Many typical marine seismic exploration sources, air-guns, boomers, etc produce a low frequency (e.g. 30 Hz in the case of air guns), short-time duration pulse which is directed into the seabed below. The resulting echo time series yields information about the structure of the earth below. Instead of using a large- peak amplitude short duration pulse, another approach ([1]-[3]) is to use an extended time-frequency pulse such as a Chirp or pseudo-noise signals. The received time series is then match-filtered to regain the time-resolution and signal-to-noise ratio. An advantage of using an extended pulse, is that its peak amplitude can be lower than that of the impulsive waveform due to the gains achieved by the matched-filtering.

In seismic surveys it is often desired to obtain echoes from reflectors several hundreds of metres deep or more. One of the limiting factors in the propagation is the attenuation within the layers. This attenuation in the simplest model is defined as a dB loss per wavelength so that the effect of the attenuation increases with frequency (see, for example, Ref. 4 for a discussion of various attenuation definitions). Some fundamental questions which can be addressed through modelling are: (1) what are the relative performances of using a low-frequency impulsive source and using an extended-time pulse in approximately the same frequency range followed by matched filtering and (2) what is the degradation in performance as the dominant frequency of the source increased and (3) how does the layer resolution depend upon the frequency content of the source. In addition, modelling can be used to study signal processing issues such as minimizing sidelobes (from the matched filtering) and beamforming (although we do not investigate beamforming in this report).

The numerical model that is developed is based upon a wavenumber integral representation of wave propagation[3]. It is formulated for a single frequency but then can be run for a set of frequencies. The earth model consists of water layer (with or without an upper air surface) and a layered elastic bottom. The reflected field at each horizontal wavenumber and the reflected field in the spatial domain is computed by performing a wavenumber integral. The time domain response is computed from Fourier synthesis of the frequency responses. Other authors [4-6] have developed numerical codes for this type of problem. The code used in this paper is a simple-to-use MATLAB implementation that we developed on the basis of the theory outlined in, for example, Refs.6 and 7. The development of this implementation has the advantages that it will be easy to adapt in the future for different modelling. Due to the fact that the code is written in MATLAB also allows one to easily include MATLAB graphical and built-in function capabilities.

We first describe the model that we have implemented and then we generate sets of time series as a function of receiver horizontal offset for different short and extended pulse types. In the case of the extended pulse types (Chirp pulses) the resulting time

series are the matched filtered, the analytic signal computed from the Hilbert Transform, and the amplitude of the envelope displayed. Layered geoacoustic models with and without attenuation are considered. In addition our model is formulated to easily compute the response with and without the effects of the upper water/air interface. In addition, the direct arrivals can also be excluded so as to better emphasize the reflection echoes.

2 Acousto-elastic modelling

We will consider a cylindrical coordinate system (r, z, θ) (z decreases for increasing depth into the Earth) and we will consider a compressional potential ϕ and a shear potential ψ [5-7] where the particle displacements $\vec{u}$ are given by

$$\begin{aligned} \vec{u} &= \nabla\phi \\ \vec{u} &= \nabla \times \nabla \times (0, 0, \psi). \end{aligned} \tag{1}$$

Within a constant-velocity elastic layer the functional form of the potentials is given by (for zero'th azimuthal order):

$$\begin{aligned} \phi &= J_0(k_x r)(A^- exp(-i\sqrt{(\omega/c_p)^2 - k_x^2}z) + A^+ exp(i\sqrt{(\omega/c_p)^2 - k_x^2}z) \\ \psi &= J_0(k_x r)(B^- exp(-i\sqrt{(\omega/c_s)^2 - k_x^2}z) + B^+ exp(i\sqrt{(\omega/c_s)^2 - k_x^2}z) \end{aligned} \tag{2}$$

where k_x is a particular horizontal wavenumber and J_0 is the Bessel Function of zero'th order. The layer-potential coefficients A^-, A^+, B^-, and B^+ will be determined by the continuity equations imposed ta the top and the bottom of the layer. It can be seen from Eq.(2) that for $k_x > \omega/c_p$ or $k_x > \omega/c_s$ there are decaying or growing exponential terms. At a horizontal interface between 2 elastic media, the boundary conditions are that

$$\begin{aligned} u_r^+ &= u_r^- \\ u_z^+ &= u_z^- \\ \tau_{rz}^+ &= \tau_{rz}^- \\ \tau_{zz}^+ &= \tau_{zz}^- \end{aligned} \tag{3}$$

If, for example, the upper layer was a fluid, then there would be no shear potential in that layer and the first boundary condition of Eq.(3) would be dropped. The symbol τ denotes the stress tensor and we also will use the relations that:

$$\tau_{rz} = \mu\left(\frac{\partial u_z}{\partial r} + \frac{\partial u}{\partial z}\right) \tag{4}$$

$$\tau_{zz} = \lambda\nabla^2\phi + 2\mu\frac{\partial u_z}{\partial z} \tag{5}$$

Using these definitions determines the 4 boundary conditions in terms of the 4 unknown coefficients above and the 4 coefficients below the interface,

$$R_j^- \begin{pmatrix} A_j^+ \\ A_j^- \\ B_j^+ \\ B_j^- \end{pmatrix} = R_{j+1}^+ \begin{pmatrix} A_{j+1}^+ \\ A_{j+1}^- \\ B_{j+1}^+ \\ B_{j+1}^- \end{pmatrix} \tag{6}$$

The expressions for the elements of the matrices R_j^- and R_j^+ are derived in the Appendix.

The coefficients for layer j as defined in Eq.(6) include the exponential vertical factors (since we evaluated the expressions as if the interface was at $z = 0$). However, a layer has a vertical thickness Δz. The values of the coefficients at the bottom of the layer $(\vec{a}_j)_B$ can be related to those at the top of the layer $(\vec{a}_j)_T$ by

$$(\vec{a}_j)_B = \begin{pmatrix} \exp(-i\Delta z\gamma_p) & 0.0 & 0.0 & 0.0 \\ 0.0 & \exp(i\Delta z\gamma_p) & 0.0 & 0.0 \\ 0.0 & 0.0 & \exp(-i\Delta z\gamma_s) & 0.0 \\ 0.0 & 0.0 & 0.0 & \exp(i\Delta z\gamma_s) \end{pmatrix} (\vec{a}_j)_T \qquad (7)$$

The expressions γ_p and γ_s denote the vertical square root factor in the exponentials of Eq.(2). The problem with Eq.(7) arises when the exponentials grow and this can be the case for A^- and B^-, when the square roots in the exponentials have a positive imaginary part. If the layer coefficients A^+ and B^+ are defined in terms of their values at the top of the layer and A^- and B^- are defined in terms of their values at the bottom of the layer, then the resultant equations for the coefficients will contain only decaying exponentials.

Let us consider a stack of N elastic layers bounded above by a water halfspace and below by an elastic basement. There are a total of 4N + 1 (water) + 2 (basement) unknowns. In the water we assume we have the specified downward incident field and the unknown upward compressional coefficient. In the basement there are the unknown downgoing compressional and shear coefficients. For N layers there are N elastic interfaces resulting in 4N equations. At the water/elastic interface there are 3 equations, resulting in a total of 4N+3 equations in 4N+3 unknowns. At the water/elastic seabed, the downward compressional coefficient d_p is specified. Thus we take the column of the equation matrix in the water, corresponding to the downward wave, multiply it by $-d_p$ and consider this as the right-hand side in a system of equations. The solution of the system of equations yields a vector of coefficients. It is the coefficient corresponding to the upward compressional coefficient in the water column which is of interest; for an incident coefficient of unity this yields $R(k_x;\omega)$, the reflection coefficient at a given wavenumber k_x and at a frequency ω. Let us suppose the incident coefficient for a point source is given by

$$\frac{\exp(i\gamma_p(k_x)z_s)}{2i\gamma_p}, \qquad (8)$$

then the spatial reflected wavefield in the water column is given by

$$p(r, z_r) = \frac{1}{2\pi}\int_0^\infty J_0(k_x r)\frac{R(k_x;\omega)}{2i\gamma_p}\exp(i\gamma_p(z_s + z_r))k_x dk_x. \qquad (9)$$

This integral has square root singularities and possibly poles along the real-axis. In order to avoid this problem we displace the contour of integration slightly down the imaginary axis in the complex-plane. In particular, we define

$$k_x(t) = t - i\epsilon \sin(\pi t/t_{end}) \tag{10}$$

and

$$dk_x(t) = (1 - i\epsilon \frac{\pi}{t_{end}} \cos(\pi \frac{t}{t_{end}}))dt \tag{11}$$

where ϵ is typically small and t_{end} is the largest value of t considered. We typically set $t_{end} = \alpha 2\pi f/c_w$ where α is a factor greater than one and c_w is the sound speed of the water column. The integral of Eq.(9) is numerically discretized using the trapezoidal rule with discrete values of t, $\{t_j\}, j = 1, ..., N_t$. Considering the discretized integrand of Eq.(9) without the Bessel function as a vector $\vec{v}$ (for fixed source and receiver depths) and considering the Bessel function has a $N_r \times N_t$ matrix B where N_r are the number of receiver ranges, then the integral can be written for multiple receiver ranges as

$$p(r_j, z_r, z_s) = B\vec{v}. \tag{12}$$

This is the reflected field - the spectral contribution for the direct field $\exp(i\gamma_p|z_r - z_s|)/(2i\gamma_p)$ can added into $\vec{v}$ or the direct term

$$\exp(i\omega/c\sqrt{r^2 + (z_r - z_s)^2})/(4\pi\sqrt{r^2 + (z_r - z_s)^2}) \tag{13}$$

can be added to the final result.

Thus far the source is in an infinite upper water halfspace. In reality, this halfspace is bounded above by the water/air interface. To include this effect, the effective field incident upon the bottom now becomes in the wavenumber representation,

$$\frac{(\exp(i\gamma_p z_s) - \exp(i\gamma_p(2h - z_s))}{i\gamma_p} \tag{14}$$

where h is the depth of the water column. For $R(k_x)$ the reflection coefficient in the water without an upper interface, the new effective reflection coefficient with the upper interface is given by

$$R - R\exp(i2\gamma_p h)R + R\exp(i2\gamma_p h)R\exp(i2\gamma_p h)R + ... = \frac{R}{1 + \exp(i2\gamma_p h)R}. \tag{15}$$

The modified receiver term becomes

$$\exp(i\gamma_p z_r) - \exp(i\gamma_p(i\gamma_p(2h - z_r))) \tag{16}$$

Thus in this case we have a new discrete wavenumber spectral vector $\vec{v}$ but the large Bessel function matrix B of Eq.(12) is the same as for the no upper interface case.

Layer	$c_p(m/s)$	$c_s(m/s)$	$\rho(g/cm^3)$	$\alpha_p(dB/\lambda)$	$\alpha_s(dB/\lambda)$	H(m)
Water	1500	–	1	0.0	0.0	(100m)
Layer 1	1750	400	1.3	0.0 (.3)	0.0 (.6)	50m
Layer 2	2100	800	1.8	0.0 (.1)	0.0 (.25)	20m
Layer 3	2300	1000	2.0	0.0 (.1)	0.0 (.25)	500m
Basement	3000	1200	2.4	0.0 (.1)	0.0 (.2)	–

Table 1: *The geoacoustic parameters used in the modelling of this report*

The final outputs from this modelling program are two-dimensional matrices of frequencies and receiver ranges: (a) one matrix is the reflected field for no upper interface and (b) one matrix includes the effects of the upper interface and the direct arrival. In the case of the direct (range = R_D) and surface-reflected direct arrival (range = R_S) the known analytical expression

$$-(\frac{\exp(i\omega/c_w R_D)}{4\pi R_D} - \frac{\exp(i\omega/c_w R_S)}{4\pi R_S}) \tag{17}$$

is used with c_w denoting the water sound speed. These matrices can then be processed by other programs which combine them with specified source functions and produce range/time series.

3 Numerical Examples

For the numerical examples of this report, the geoacoustic parameters are listed above in Table 1. In this table c_p denotes the compressional sound speed of the layer, c_s, the shear speeds, ρ the densities, α_p and α_s, the compressional and shear attenuations (if used in the computation) and finally the layer thicknesses H. The attenuations will only be used in some of the computations. There are two quite thin near-surface sediment layers followed by a thick layer, terminating in a reflector at 570m depth.

For the first computations we show in Figs.1-3 the resulting transmission loss curves as computed by the method of this report and by OASES[2] for frequencies ranging from 0.25 to 32 Hz. The wavenumber integrals are computed out to the maximum $(10\omega/1500, 0.2)$ for each frequency with 20000 discretization points. The geoacoustic parameters of Table I with the attenuations are used. For these computations $\epsilon = 0.001$. There are some very small differences between the 2 curves for the low frequencies - the overall agreement of all curves is excellent (it should be noted that the agreement is so good that the curves may appear indistinguishable in the figures).

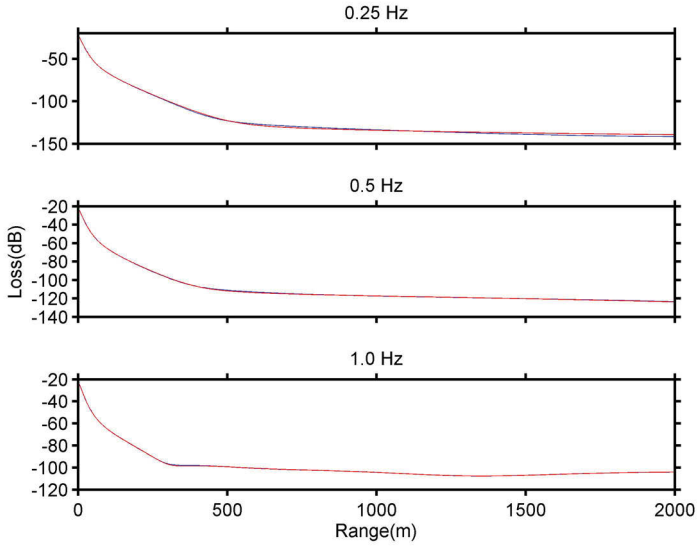

Figure 1: *Transmission Loss curves OASES (blue), MATLAB code (red) for frequencies of 0.25 to 1 Hz. The 2 lines, blue and red, are difficult to distinguish due to their very close agreement.*

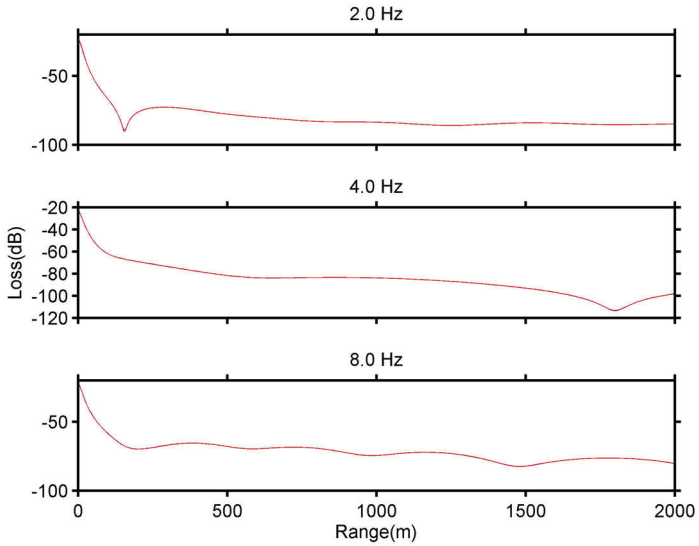

Figure 2: *Transmission Loss curves OASES (blue), MATLAB code (red) for frequencies of 2 to 8 Hz. The 2 lines, blue and red, are difficult to distinguish due to their very close agreement.*

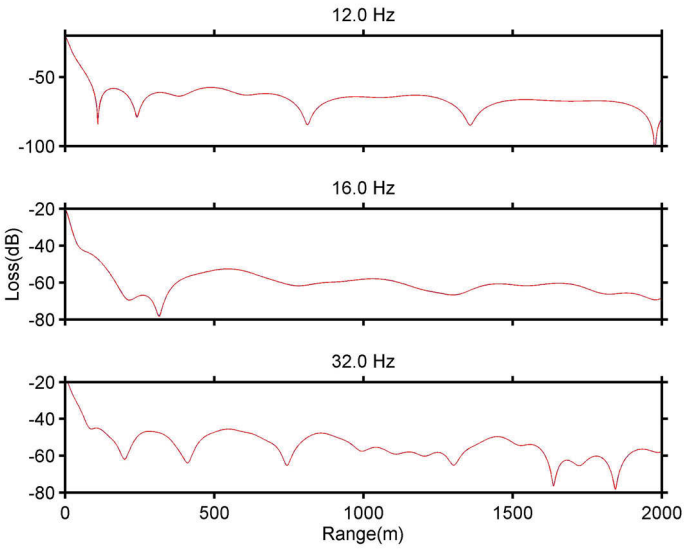

Figure 3: *Transmission Loss curves OASES (blue), MATLAB code (red) for frequencies of 12 to 32 Hz. The 2 lines, blue and red, are difficult to distinguish due to their very close agreement.*

We now compute the time-domain responses for 400 ranges between 5 and 2000 m and 4096 frequencies between 0 and $4095 \times 0.125Hz$ (the 0 frequency is reset to 0.05 Hz). The source and receivers are 90 m and 80 m above the seabed (or 10m and 20m depth respectively when the upper wate/air interface is included) . The fine frequency sampling means that in the time domain we can compute out to 8 seconds in duration. A value of $\epsilon = 0.004$ was used to offset the contour in these computations. In Fig.4 we show the direct arrival pulses as computed at the horizontal distance of 505 m (trace 101) for the three different pulse types considered in this report. the first pulse type is a 30-Hz Ricker pulse. The second type is a Chirp pulse with length T of 2 seconds and we consider first a frequency sweep between 10 and 70 Hz and then a sweep between 50 and 250 Hz. These Chirps are tapered with a Tukey window (i.e., split cosine bell) of fraction 0.5. The source spectra are normalized such that in the time domain the sum of squares of the corresponding signal is equal to unity.

$$S(t) = sin(2\pi t(f_0 + \frac{\Delta f t}{2T})), \quad 0 \leq t \leq T \tag{18}$$

It can be seen that to contain the same amount of energy, the longer Chirp pulses have a peak amplitude of less than 20% of that of the impulsive Ricker pulse. The propagation computations are such that in the frequency domain the direct arrival has the form $-\frac{\exp(i\omega/c_w R)}{4\pi R}$. In Figs. 5-7 we show the computed seismic sections for the three pulse types (be seismic section, we simply mean the time-horizontal off set image). For the Chirp pulses, the results are the amplitude of the envelope of the

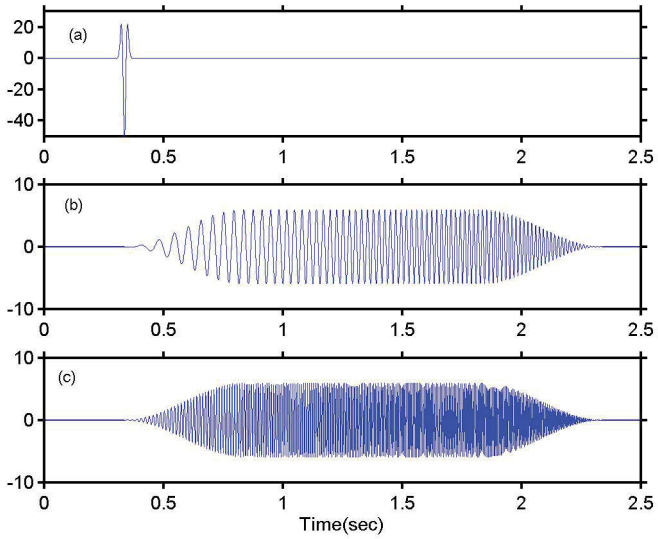

Figure 4: *Three pulse types: (a) Ricker wavelet (30Hz) (b) tapered 10-70 Hz Chirp (c) tapered 50-250 Hz Chirp. For display purposes, they have all been multiplied by a factor of 1.E6*

match-filtered output. For the matched filtering the known incident pulse is used as the replica. These sections do not include the effects of the upper water/air interface or the direct arrival which would further complicate the time history.

The resulting seismic sections are qualitatively similar to each other and have similar amplitudes, although the broader band image of Fig.7 shows some more detail. There is a time offset with the matched-filtering results due to the half-width of the template signal which we have accounted for. Also, for the higher-frequency/larger bandwidth section of Fig.7, there is an arrival at the larger offsets (starting at approximately 1000m) which is not observable in the lower frequency results of Figs.5 and 6. This corresponds to the combination of the single reflection off the interface at 50m depth (bottom of the first sediment layer) and the multi-path consisting of an upper reflection off the seabed/layer 1 interface and two reflections off the 50m interface. These 2 echoes arrive very close in time at the longer ranges and at lower frequencies destructively interfere - at the larger bandwidth they start to become resolvable.

In comparison with Fig.5, we show in Fig. 8 the seismic section for the Ricker wavelet when the direct arrival and all the interactions with the upper water/air interface are modelled. It can be seen that the interpretation of the section in terms of arrivals from reflectors and those which are air-surface/seabed multiples is difficult. In addition, the relative closeness of the source and receiver (10 and 20m respectively) to the upper surface means that there are 4 paths associated with each reflection, i.e., direct

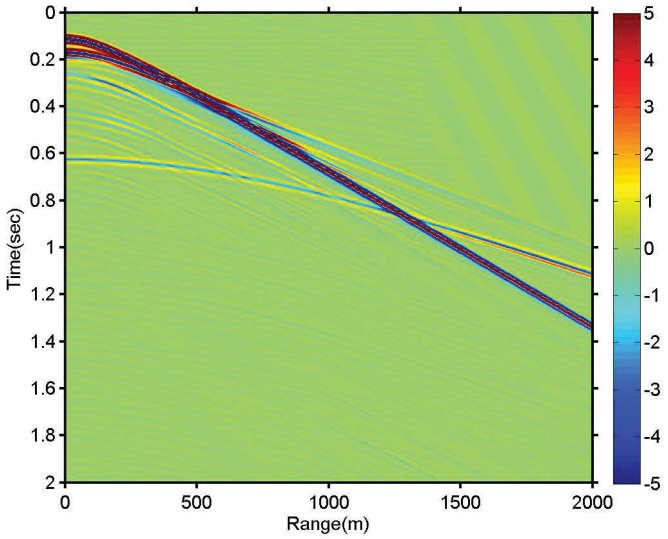

Figure 5: *The seismic section for the 30-Hz Ricker wavelet - top surface and direct arrival not included. The values have been multiplied by 1.E6*

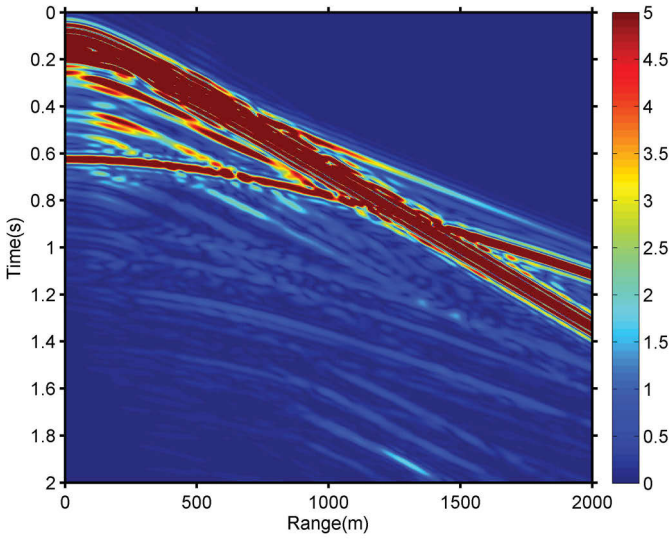

Figure 6: *The seismic section for the Chirp 10-70 Hz (2 seconds). The absolute value of the envelope of the match-filtered output is shown after multiplication by 1.E6.*

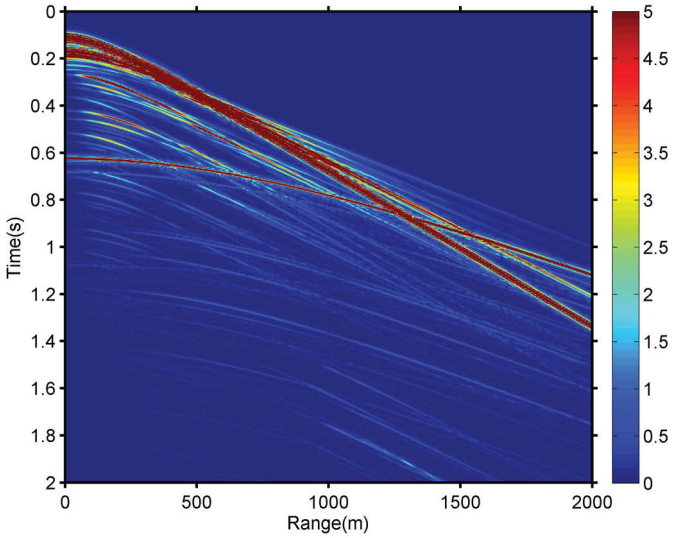

Figure 7: *The seismic section for the Chirp 50-250 Hz (2 seconds). The absolute value of the envelope of the match-filtered output is shown after multiplication by 1.E6*

incidence/direct receive, one surface reflection incidence/ direct receive, direct incidence/one surface reflection receive, and one surface reflection incidence/one surface reflection receive.

We now implement the attenuations listed in Table I. The resulting reflection seismic section for the 50-250 Hz Chirp is shown in Fig.9. The resulting reflection seismic section is similar to the no attenuation sections of Fig.7 but with many arrivals now significantly lower in amplitude. However, the arrival from the reflector at 570m depth is still evident.

Finally, we show some of the individual time series (traces) in more detail. In Fig.10 two traces, with the Ricker and the 2 Chirps (after matched filtering) are shown for a near hydrophone (55 m horizontal separation) and the farthest hydrophone (2000 m separation). These are for the case of no attenuation. For trace 11 of Fig.10, the first echo is from the seabed and this is evident for all 3 pulse types. The second echo corresponds to the first interface at 50m depth combined with the third interface 20m further in depth. This interface is not distinguishable in the case of the Ricker and the 10-70 Hz Chirp, but is distinct for the wider bandwith 50-250 Hz Chirp. The echo from the lowest interface at 570 m depth is received at approximately 0.6 seconds and is evident or all 3 pulses. At the far hydrophone, the echo from the deepest interface arrives first and the seabed reflection is at about 1.35 seconds. In Fig.11 the same results are shown but now with attenuation included in the layers. As

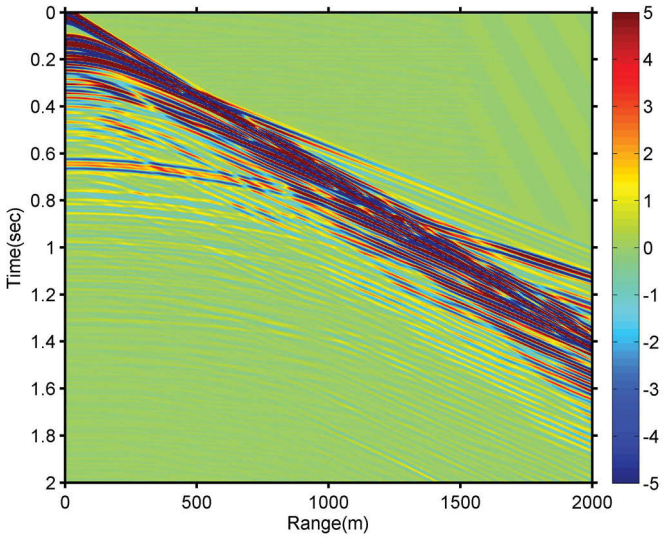

Figure 8: *The seismic section for the Ricker wavelet with direct arrival and upper surface interactions included. The results are shown after multiplication by 1.E6*

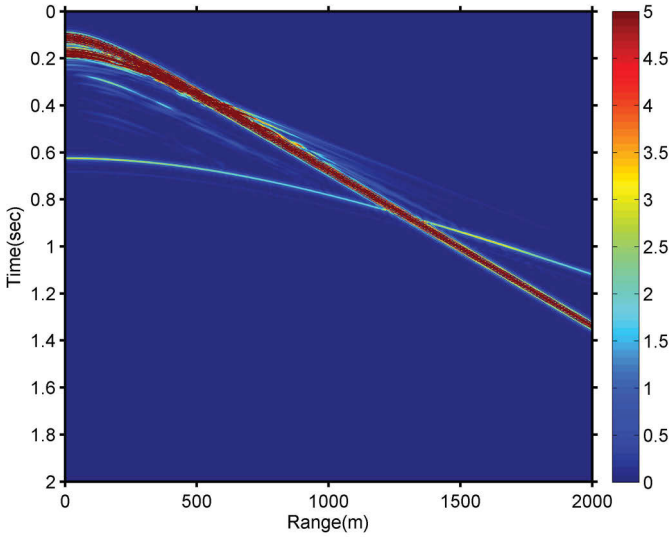

Figure 9: *The seismic section for the 50-250 Hz Chirp (direct arrival and upper surface interactions not included). The attenuations of Table 1 are considered. The results are shown after multiplication by 1.E6*

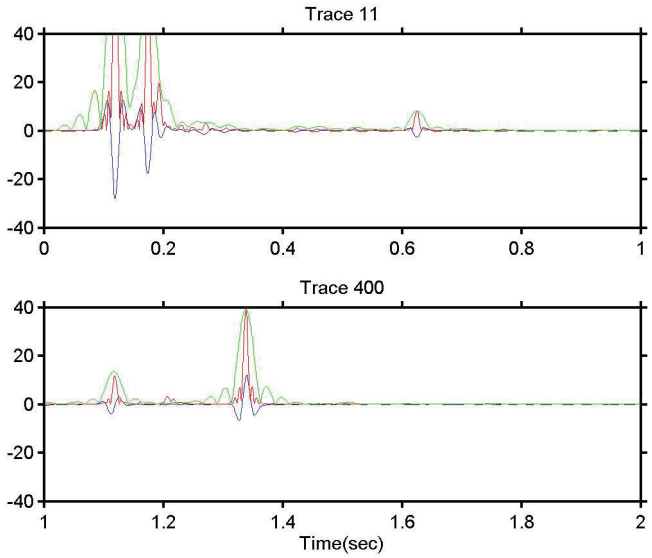

Figure 10: *The Ricker wavelet (blue) and the two matched-filtered results 10-70 Hz(green) and 50-250 Hz(red) for the hydrophones at 55 and 2000 m horizontal separation. There is no attenuation. The results are shown after multiplication by 1.E6*

would be expected the echoes from the seabed and the shallower interfaces are largely unaffected by the inclusion of attenuation. For the 50-250 Hz pulse the reflection from the interface at 570m is significantly weaker.

An advantage of the impulsive Ricker wavelet is that the phase of the reflection is visually evident. For example, for Trace 11 the polarity of the reflected Ricker pulses from the seabed and the layer at 50m depth are the same as the incident pulse, whereas the reflection of Trace 400 at about 1.4 seconds has approximately the reverse polarity. In the case of the match-filtered results the phase of the reflections are not observable.

4 Discussion of Results

We have written a MATLAB program for the computation of reflection time series in a horizontally layered geoacoustic medium. This code is similar in its formulation to other numerical codes. However, because it is written in MATLAB it is easily incorporated with the other MATLAB routines and graphics. In addition, it can be easily modified in the future to meet additional modelling requirements.

Using this code, the time series for an array of receivers and for different pulses were

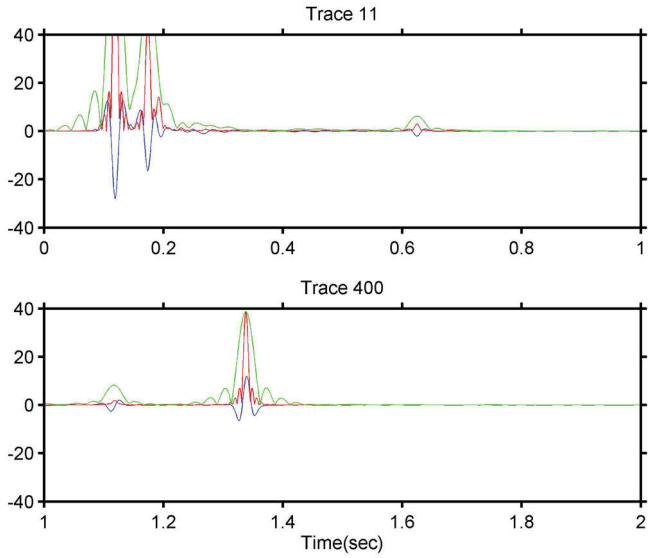

Figure 11: *The Ricker wavelet (blue) and the two matched-filtered results 10-70 Hz(green) and 50-250 Hz(red) for the hydrophones at 55 and 2000 m horizontal separation. The attenuations have been included. The results are shown after multiplication by 1.E6*

computed. In the case of long extended pulses, the outputs were match-filtered with a resulting increase in output amplitude and a compression in time. This type of modelling allows one to investigate the effects of centre, frequency, bandwidth, and medium attenuation. In addition, one can also consider various signal processing issues such as tapering the pulse to reduce sidelobe levels in the matched-filtering. One could also consider more advanced deconvolution techniques to improve the resolution of the resulting seismic sections.

Annex A: Details of the scattering matrix R

In this appendix we give the detailed formulas for the elements of the scattering matrix R described in Section 2. In particular, we utilize the 4 elastic continuity equations in terms of downward and upward-going compressional and shear potentials. Let use take the upward compressional potential ϕ^+ as $A^+ J_0(k_r r)\exp(i\sqrt{(\frac{\omega}{c})^2 - k_r^2})$, the downward compressional potential as $A^- J_0(k_r r)\exp(-i\sqrt{(\frac{\omega}{c})^2 - k_r^2})$ and similarly for the shear potentials in terms of B^+ and B^-. Then for the displacements and stresses we obtain (evaluated for $z = 0$):

$$\begin{aligned} u_r &= \frac{\partial \phi}{\partial r} + \frac{\partial^2 \psi}{\partial r \partial z} && \text{(A.1)} \\ &= -k_r(A^+ + A^- + i\gamma_s B^+ - i\gamma_s B^-)J_1(k_r r) && \text{(A.2)} \end{aligned}$$

The $k_r J_1(k_r r)$ term, arising from the radial derivative of the potentials is common to all terms for u_r and can be ignored. For the vertical displacement u_z one obtains

$$\begin{aligned} u_z &= \frac{\partial \phi}{\partial z} - \frac{1}{r}\frac{\partial}{\partial r} r \frac{\partial \psi}{\partial r} && \text{(A.3)} \\ &= (i\gamma_p(A^+ - A^-) + k_r^2(B^+ + B^-))J_0(k_r r) && \text{(A.4)} \end{aligned}$$

For the stresses we have that

$$\begin{aligned} \sigma_{rz} &= \mu(\frac{\partial u_r}{\partial z} + \frac{\partial u_z}{\partial r}) && \text{(A.5)} \\ &= \mu(2\frac{\partial^2 \phi}{\partial r \partial z} + \frac{\partial^3 \psi}{\partial z^2 \partial r} + k_r^2 \frac{\partial \psi}{\partial r}) && \text{(A.6)} \\ &= -k_r \mu(2i\gamma_p A^+ - 2i\gamma_p A^+ + (2k_r^2 - \omega^2/c_s^2)(B^+ + B^-))J_1(k_r r) && \text{(A.7)} \end{aligned}$$

and

$$\begin{aligned} \sigma_{zz} &= \lambda \nabla^2 \phi + 2\mu \frac{\partial u_z}{\partial z} && \text{(A.8)} \\ &= -\lambda\omega^2/c_p^2 \phi + 2\mu(\frac{\partial^2 \phi}{\partial z^2} + k_r^2 \frac{\partial \psi}{\partial z}) && \text{(A.9)} \\ &= ((-\lambda\omega^2/c_p^2 - 2\mu\gamma_p^2)(A^+ + A^-) + 2\mu k_r^2 i\gamma_s(B^+ - B^-))J_0(k_r r) && \text{(A.10)} \end{aligned}$$

From these expressions we can construct the matrices R_j^+ and R_j^- discussed in Section 2. From the expressions above, we obtain for R (the superscript + would use medium parameters for the upper medium and -, medium parameters for the lower medium)

$$\begin{pmatrix} 1 & 1 & i\gamma_s & -i\gamma_s \\ i\gamma_p & -i\gamma_p & k_r^2 & k_r^2 \\ 2i\gamma_p & -2i\gamma_p & (2k_r^2 - \omega^2/c_s^2) & (2k_r^2 - \omega^2/c_s^2) \\ -\lambda\omega^2/c_p^2 - 2\mu\gamma_p^2 & -\lambda\omega^2/c_p^2 - 2\mu\gamma_p^2 & 2\mu k_r^2 i\gamma_s & -2\mu k_r^2 i\gamma_s \end{pmatrix} \quad \text{(A.11)}$$

Here we have used the same notation as in Section 2.

References

[1] S. G. Shhock, L.R. LeBlanc, and L.A. Mayer, "Chirp subbottom profiler for quantitative sediment analysis", Geophysics, Vol.4, pp.445-450 (1989).

[2] W.H. Dragoset, "Marine vibrators and the doppler effect", Geophyscis, Vol.53, pp.1388-1398, 1988.

[3] B. Askeland, H. Hobæk, and R. Mjelde, "Marine sesimics with a pulsed combustion source and Pseudo Noise codes", Mar Geophys Res., Vol.28, pp.109-117 (2007).

[4] H. Schmidt, OASES Version 2.1 User Guide and Reference Manual, MIT, 2001.

[5] B.L.N. Kennett, *Seismic wave propagation in stratified media*, Cambridge University Press, 1983.

[6] F.B. Jensen, W.A. Kuperman, M.B. Porter, and H. Schmidt, *Computational Ocean Acoustics*, AIP Press, 1993.

[7] K. Aki and P.G. Richards, *Quantitative Seismology Theory and Methods Vol. 1*, W.H Freeman and Company, 1980.

Distribution list

Document No.: DRDC Atlantic TM 2011-236

LIST PART 1: Internal Distribution by Centre

2 DRDC Atlantic Library

2 TOTAL LIST PART 1

LIST PART 2: External Distribution by DRDKIM

1 NDHQ/DRDKIM (email pdf file)

1 TOTAL LIST PART 2

3 TOTAL COPIES REQUIRED

This page intentionally left blank.

DOCUMENT CONTROL DATA

(Security markings for the title, abstract and indexing annotation must be entered when the document is Classified or Designated.)

1. ORIGINATOR (The name and address of the organization preparing the document. Organizations for whom the document was prepared, e.g. Centre sponsoring a contractor's report, or tasking agency, are entered in section 8.)

Defence Research and Development Canada – Atlantic
PO Box 1012, Dartmouth NS B2Y 3Z7, Canada

2a. SECURITY MARKING (Overall security marking of the document, including supplemental markings if applicable.)

UNCLASSIFIED

2b. CONTROLLED GOODS

(NON-CONTROLLED GOODS)
DMC A
REVIEW: GCEC APRIL 2011

3. TITLE (The complete document title as indicated on the title page. Its classification should be indicated by the appropriate abbreviation (S, C or U) in parentheses after the title.)

Numerical modelling of coherent broadband pulses for seismic exploration

4. AUTHORS (Last name, followed by initials – ranks, titles, etc. not to be used.)

Fawcett, J.

5. DATE OF PUBLICATION (Month and year of publication of document.)	6a. NO. OF PAGES (Total containing information. Include Annexes, Appendices, etc.)	6b. NO. OF REFS (Total cited in document.)
November 2011	32	7

7. DESCRIPTIVE NOTES (The category of the document, e.g. technical report, technical note or memorandum. If appropriate, enter the type of report, e.g. interim, progress, summary, annual or final. Give the inclusive dates when a specific reporting period is covered.)

Technical Memorandum

8. SPONSORING ACTIVITY (The name of the department project office or laboratory sponsoring the research and development – include address.)

Defence Research and Development Canada – Atlantic
PO Box 1012, Dartmouth NS B2Y 3Z7, Canada

9a. PROJECT OR GRANT NO. (If appropriate, the applicable research and development project or grant number under which the document was written. Please specify whether project or grant.)	9b. CONTRACT NO. (If appropriate, the applicable number under which the document was written.)
11CJ56	

10a. ORIGINATOR'S DOCUMENT NUMBER (The official document number by which the document is identified by the originating activity. This number must be unique to this document.)	10b. OTHER DOCUMENT NO(s). (Any other numbers which may be assigned this document either by the originator or by the sponsor.)
DRDC Atlantic TM 2011-236	

11. DOCUMENT AVAILABILITY (Any limitations on further dissemination of the document, other than those imposed by security classification.)

(X) Unlimited distribution
( ) Defence departments and defence contractors; further distribution only as approved
( ) Defence departments and Canadian defence contractors; further distribution only as approved
( ) Government departments and agencies; further distribution only as approved
( ) Defence departments; further distribution only as approved
( ) Other (please specify):

12. DOCUMENT ANNOUNCEMENT (Any limitation to the bibliographic announcement of this document. This will normally correspond to the Document Availability (11). However, where further distribution (beyond the audience specified in (11)) is possible, a wider announcement audience may be selected.)

13. ABSTRACT (A brief and factual summary of the document. It may also appear elsewhere in the body of the document itself. It is highly desirable that the abstract of classified documents be unclassified. Each paragraph of the abstract shall begin with an indication of the security classification of the information in the paragraph (unless the document itself is unclassified) represented as (S), (C), or (U). It is not necessary to include here abstracts in both official languages unless the text is bilingual.)

As part of the Offshore Energy Environmental Research (OEER)/DRDC Atlantic project "Feasibility of a Marine Vibroseis System to Minimize Potential Impacts of Seismic Surveying on Commercial Marine Invertebrates", DRDC Atlantic has been investigating the possibility and technical feasibility of using coherent broadband sources with complex waveforms (followed by matched-filtering) to replace high amplitude impulsive sources used in marine seismic surveys. This report discusses a MATLAB implementation of an acousto-elastic wavenumber algorithm for layered geoacoustic media. This code is then used to generate broadband time series for different geological configurations and incident waveforms. The relative performances of different impulsive and extended-time broadband sources are investigated. As well, the effects of the upper air/water interface and the inclusion of attenuations in the elastic layers are modelled.

14. KEYWORDS, DESCRIPTORS or IDENTIFIERS (Technically meaningful terms or short phrases that characterize a document and could be helpful in cataloguing the document. They should be selected so that no security classification is required. Identifiers, such as equipment model designation, trade name, military project code name, geographic location may also be included. If possible keywords should be selected from a published thesaurus. e.g. Thesaurus of Engineering and Scientific Terms (TEST) and that thesaurus identified. If it is not possible to select indexing terms which are Unclassified, the classification of each should be indicated as with the title.)

seismic, modelling

This page intentionally left blank.

Defence R&D Canada

Canada's leader in defence
and National Security
Science and Technology

R & D pour la défense Canada

Chef de file au Canada en matière
de science et de technologie pour
la défense et la sécurité nationale

DEFENCE DÉFENSE

www.drdc-rddc.gc.ca